

# Mutual Adaptation in Human-Robot Co-Transportation with Human Preference Uncertainty

Al Jaber Mahmud, Weizi Li, and Xuan Wang

**Abstract**—Mutual adaptation can significantly enhance overall task performance in human-robot co-transportation by integrating both the robot’s and human’s understanding of the environment. While human modeling helps capture humans’ subjective preferences, two challenges persist: (i) the uncertainty of human preference parameters and (ii) the need to balance adaptation strategies that benefit both humans and robots. In this paper, we propose a unified framework to address these challenges and improve task performance through mutual adaptation. First, instead of relying on fixed parameters, we model a probability distribution of human choices by incorporating a range of uncertain human parameters. Next, we introduce a time-varying stubbornness measure and a coordination mode transition model, which allows either the robot to lead the team’s trajectory or, if a human’s preferred path conflicts with the robot’s plan and their stubbornness exceeds a threshold, the robot to transition to following the human. Finally, we introduce a pose optimization strategy to mitigate the uncertain human behaviors when they are leading. To validate the framework, we design and perform experiments with real human feedback. We then demonstrate, through simulations, the effectiveness of our models in enhancing task performance with mutual adaptation and pose optimization.

## I. INTRODUCTION

Human-robot collaboration (HRC) has gained increasing attention in research due to its potential to enhance efficiency and safety in daily tasks where robots can operate in close proximity to humans. Achieving seamless cooperation requires robots to understand human behavior and anticipate the inherent uncertainties in human decision-making. Classical cognitive and behavioral models offer theoretical frameworks to capture human biases, heuristics, and risk attitudes [2]–[4]. However, the effectiveness of these models depends on accurately identifying model parameters, which is often challenging, as they may vary among individuals and fluctuate even for the same individual under different experimental conditions. On the other hand, data-driven and learning-based approaches [5], [6] have demonstrated success in modeling human behavior. However, deep neural networks, commonly used in such methods, often suffer from limited explainability and generalizability. Despite extensive research on predicting and understanding human behavior, only a limited number of studies [7]–[9] integrate human behavior modeling into low-level robot control during collaboration. Moreover, existing works [8], [9] typically focus on static, one-time interactions rather than considering dynamic, evolving environments.

In this work, we consider a co-transportation task (Fig. 1), where a human-robot team must navigate from a start posi-

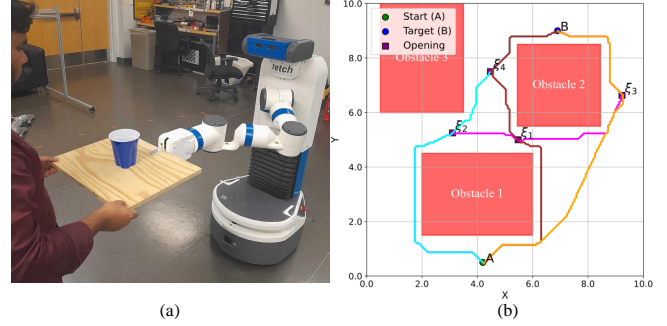


Fig. 1: (a) Task: Human-Robot Co-Transportation. (b) Environment: Navigating through obstacles to the target. There exist multiple path options to reach. In some options, there is a high risk of collision (e.g.,  $A \rightarrow \xi_1 \rightarrow \xi_4 \rightarrow B$ ), or with some options, the team needs to traverse a longer distance (e.g.,  $A \rightarrow \xi_3 \rightarrow B$ ).

tion to a target through the *openings* of multiple obstacles. Throughout this process, variations in human preferences can significantly influence path selection. If the robot fails to account for these preferences, task performance may degrade, potentially leading to failure. Unlike existing research, we focus on two unique aspects of this problem: (i) accounting for the uncertainty in human preference parameters and (ii) introducing a time-varying stubbornness measure that dynamically evolves as the task progresses. Driven by these, we propose a framework that integrates human modeling, human-robot interaction analysis, and the robot’s low-level control. The main contributions of this work include:

- A mathematical model of human preferences that captures uncertainties in human parameters regarding their perceptions of risk and distance across multiple options. The model generates probability distributions that represent the likelihood of human decision on each choice.
- A time-varying stubbornness measure, integrated with probability distributions of human decisions into a coordination mode transition model for team decision-making. This enables both the human and the robot to adapt to each other dynamically over time.
- A pose optimization strategy that accounts for potential deviations in human behavior, allowing the robot to proactively mitigate the impact of unexpected changes in human decisions while ensuring safe and efficient object transportation.

## II. LITERATURE REVIEW

Human-robot collaboration emerges when both humans and robots share both a goal and a common object, thus demanding more rigorous safety measures for both the human and the manipulated object. This include wood sawing

A. Mahmud and X. Wang are with George Mason University. W. Li is with the University of Tennessee, Knoxville. Supplementary material of this work can be found at [1].

and surface polishing [9], co-transportation tasks [10], [11], and object manipulation tasks [12].

*Human Behavior Model:* Understanding human behavior in human-robot collaboration can improve the efficiency and safety of the task. Various methods, including deep learning [5], reinforcement learning [13], and spiking neural networks [6] have been employed to learn human behaviors from data. However, these data-driven approaches often lack interpretable mathematical frameworks that describe the inherent decision-making processes in humans. Classical cognitive and behavioral models, such as prospect theory [2], Prelec’s probability weighting function [4], Steven’s power law [3], drift-diffusion models [14], and Bayesian models [15], provide theoretical structures to capture human perception and decision-making. Yet, these models often end up with specific human parameter values that may not be accurate across different individuals performing the same task [16]. Furthermore, humans may initially be willing to adapt, but if they capture continuous disagreement, they can become more resistant in adapting to the robot [17].

*Mutual Adaptation:* To analyze the adaption modes in human-robot collaboration, many studies have focused on *single-direction robot adaptation* to human actions. Such approaches include co-transportation [11], co-manipulation tasks [9], [18], robot learning from demonstrations [19], adaptive motion planning under uncertainties [20], human-robot handovers [21], and adaptive task planning in shared environments [22]. Similarly, there exist *single-direction human adaptation* methods, where the robot leads while the human adapts, such as in robotic tour-guiding [23] and complex navigation assistance [24]. Although single-direction adaptation is sufficient for some tasks, it may cause human discomfort or disengagement [25], riskier task approaches, or longer execution times [26]. Such drawbacks highlight the need for *mutual adaptation* between the human and the robot for enhanced efficiency in collaboration [8], [27], in particular incorporating the modern human modeling techniques mentioned above.

*Pose Optimization:* Despite incorporating human variability and behavioral change, mathematical models cannot perfectly capture every individual’s behavior and decision-making processes [16], [28]. Consequently, robots must be prepared to handle uncertainties and unexpected human choices. Although previous studies have discussed human uncertainty in decision-making [29]–[31], adapting robots at low-level control to unexpected human choices remains a substantial challenge. For such low-level control in the robot’s end-effector, the idea of pose optimization, which is related to redundancy resolution [32], [33], helps to avoid kinematic singularities [34], improving the overall reachability of the robot manipulator [35]. Our previous work [36] has explored this strategy; however, it did not explicitly integrate a human behavioral model with a probabilistic distribution of human choices. Hence, there is a need for a more unified approach that combines human behavior modeling with uncertain human parameters, the mutual adaptation among humans and robots, and pose optimization to ensure safe, effective, and comfortable collaboration.

### III. PRELIMINARIES AND PROBLEM FORMULATION

#### A. The Co-transportation Task and Path Selection

In this paper, we consider a co-transportation task in which a human and a robot jointly transport an object from a start position to a target position. As illustrated in Fig. 1, the environment contains several obstacles that must be avoided for navigation safety. We assume that both the human and the robot have complete knowledge of the environment. Depending on the geometric properties of these obstacles, the human-robot team will have to navigate through the ‘openings’ among obstacles, leading to multiple path options. Assuming the considered paths do not involve loops, the total number of path options is finite.

To evaluate feasible paths for the co-transportation task, we consider two factors: the collision risks  $S$  when transporting through all openings and the total traveling distances  $D$ . Specifically, let  $\Xi$  be the set of all openings. An opening  $\xi \in \Xi$  is defined as a passage between obstacles whose width satisfies  $d_r < w_\xi \leq 5d_r$ ,<sup>1</sup> where  $d_r$  is the width of the robot. The risk associated with opening  $\xi$  is quantified as

$$S_\xi = \frac{d_r}{w_\xi}, \quad (1)$$

Here  $S_\xi \in [0, 1]$  is the percentage of risk. In general, a narrower passage implies a higher risk.

A feasible path option  $o \in \mathcal{O}$  connects the system’s current position to the target point through a sequence of openings. Here,  $\mathcal{O}$  denotes the set of all path options.<sup>2</sup> Let  $\Xi_o \subset \Xi$  be the set of openings associated with option  $o$ , and the percentage of collision risk  $S_o$  for this option is then defined by the stacking of risk as:

$$S_o = 1 - \prod_{\xi \in \Xi_o} (1 - S_\xi) \quad (2)$$

Let  $D_o$  represent the total length of path option  $o$  to the target. The overall cost for option  $o$  is quantified as

$$\mathcal{J}_o = D_o + c_r \cdot S_o, \quad (3)$$

where  $c_r$  is a scalar weight that determines the relative importance of collision risk versus travel distance.

Note that (3) represents an **objective** cost that can be utilized by robots to optimize their performance by balancing between safety (risk minimization) and efficiency (distance minimization). Nevertheless, in most cases, humans perceive risks and distances subjectively, leading to a discrepancy between human and robotic evaluations, as we introduce next.

#### B. Subjective Human Cost with Risk-Distance Perception

Humans tend to exhibit nonlinear risk perception, often overestimating small risks while underestimating large

<sup>1</sup>When a passage is wider than  $5d_r$ , we assume the human-robot team can traverse it without incurring any risk. This threshold may be adjusted based on real-world scenarios.

<sup>2</sup>Note that  $\mathcal{O}$  may change dynamically, depending on the current positions of the human-robot team. Here, we introduce the generic concept of cost evaluation and omit time-step indicators.

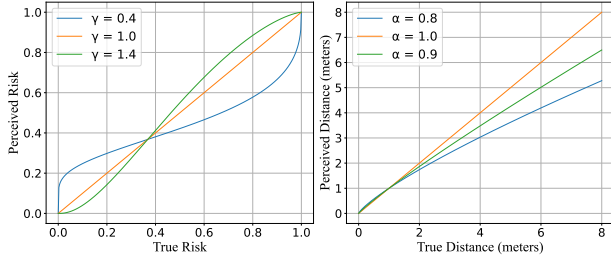


Fig. 2: True risk ( $\gamma = 1$ ) and true distance ( $\alpha = 1$ ). For perceived risk, when  $\gamma < 1$  the weighting function overemphasizes small risks and underemphasizes large risks, whereas when  $\gamma > 1$  the opposite trend is observed. Perceived distance varies with  $\alpha$ , reflecting differences in individual sensitivity.

ones [2]. To capture this phenomenon, we introduce subjective risk measure based on Prelec’s function [4],

$$\hat{S}_o = \exp\left(-(-\ln(S_o))^\gamma\right). \quad (4)$$

Here, the parameter  $\gamma$  influences the curvature of the weighting function. When  $\gamma < 1$ , humans overweight small risk probabilities and underweight large probabilities of risk. For  $\gamma > 1$ , the perception towards probabilities is the opposite.

Similarly, humans may not perceive the actual travel distance accurately. Inspired by Steven’s power law [3], [37], [38], we model an individual’s sensitivity to distance as

$$\hat{D}_o = D_o^\alpha, \quad (5)$$

where  $\alpha \leq 1$  is usually observed, reflecting that humans tend to underweight large distances. Combining these elements, the human’s **subjective** cost for an option  $o$  is defined as

$$\hat{\mathcal{J}}_o(\alpha, \gamma) = \hat{D}_o + c_r \cdot \hat{S}_o. \quad (6)$$

This function describes how humans form subjective judgments based on their own attitude toward risk (whether risk-seeking or risk-averse) and their ability to measure distance through observations. Although this model can be used to predict human decisions, setting the parameters with specific values is not guaranteed to be accurate, as they vary among individuals and even for the same individual under different experimental conditions. Thus, the uncertainties in these parameters must be taken into account.

### C. Problem of Interest

In this paper, we investigate the human-robot co-transportation task while explicitly considering the uncertainties in subjective preference parameters. To enhance robot cooperation with humans, the following research questions must be addressed. (i) Human modeling: How to quantify the uncertainties in human decision-making that arise from variations in their subjective preference parameters. (ii) Human-robot alignment: Given the uncertainties in human decision-making, how the robot aligns its behavior with the human to improve the co-transportation task. (iii) Robot control: How the human model and human-robot alignment mechanism can inform the low-level control of the robot to enhance task performance.

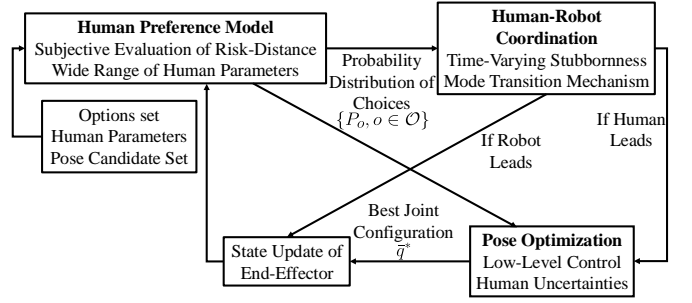


Fig. 3: Overview of our proposed mutual adaption framework in human-robot co-transportation with human preference uncertainties. The *Human Preference Model* produces a probability distribution of options. A time-varying human stubbornness measure is developed that incorporates these probabilities into a *Human-Robot Coordination Model* to determine their coordination modes. If human leads, the *Pose Optimization*, informed by these models, generates joint configurations that better prepare the robot’s low-level control to handle potential human uncertain behaviors.

## IV. MAIN APPROACH

Aligned with our problem formulation to account for human preference uncertainties, our approach to the formulated human-robot co-transportation task comprises three key components: (i) A human preference model that computes a probability distribution representing the likelihood of a human selecting a particular path option. (ii) A measure of human stubbornness that informs the mode of human-robot coordination and guides the robots in selecting paths that accommodate human preferences. (iii) A pose optimization strategy integrated into the robot’s low-level control system, which proactively compensates for uncertainties in human decision-making while the robot adapts to the human. These modules are interconnected, as illustrated by the flowchart in Fig. 3.

### A. Probability Distribution of Human Choices

In this subsection, we develop a mathematical model that maps uncertainty in human decision-making parameters into a probability distribution representing the likelihood of a human choosing a particular option.

Based on the subjective cost defined in (6), we assume the human chooses the option with the lowest subjective cost, i.e.,

$$o_h(\alpha, \gamma) = \arg \min_{o \in \mathcal{O}} \hat{\mathcal{J}}_o(\alpha, \gamma) \quad (7)$$

where  $o_h(\cdot)$  is the human preferred option, which depends on the parameters  $\alpha$  and  $\gamma$ .

To account for uncertainties of human preference parameters, we model  $\alpha$  and  $\gamma$  as two independent variables following uniform distribution<sup>3</sup> such that,

$$\alpha \sim \mathcal{U}(\underline{\alpha}, \bar{\alpha}), \quad \gamma \sim \mathcal{U}(\underline{\gamma}, \bar{\gamma}). \quad (8)$$

where  $\underline{\cdot}$  and  $\bar{\cdot}$  represent the lower and upper bound of the distribution, respectively. Hence, for each pair of  $(\alpha, \gamma)$ ,

<sup>3</sup>The results can be easily generalized to other types of distributions such as the normal distribution.

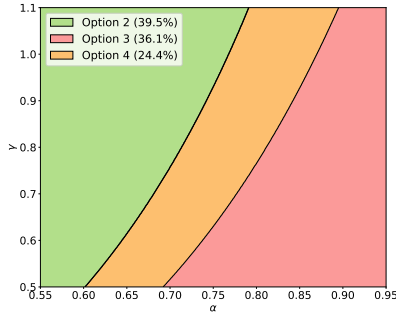


Fig. 4: With the environment in Fig. 1, the probability distribution of choosing an option based on the parameter distributions  $\alpha \sim U(0.55, 0.95)$  and  $\gamma \sim U(0.5, 1.1)$  with  $c_r = 10$ . The colored regions correspond to the lowest subjective cost of each option. The probabilities are computed based on the areas of these regions.

the human's preferred option  $o_h(\alpha, \gamma)$  may differ, leading to a distribution over the preferred options. As illustrated in Fig. 4, this partitions the  $(\alpha, \gamma)$  plane into regions  $\mathcal{R}_o$  defined as:

$$\mathcal{R}_{o_h} = \{(\alpha, \gamma) \mid o_h\}. \quad (9)$$

Given the uniform distributions for  $\alpha$  and  $\gamma$ , the probability that the human chooses option  $o$  is formulated as the ratio of the area of  $\mathcal{R}_o$  to the total area of the parameter space:

$$P_{(o=o_h)} = \frac{1}{(\bar{\alpha} - \underline{\alpha})(\bar{\gamma} - \underline{\gamma})} \iint_{\mathcal{R}_{o_h}} d\alpha d\gamma. \quad (10)$$

Thus, our model yields a probability distribution over the set of options,  $\{P_o, o \in \mathcal{O}\}$ , allowing the robot to anticipate variability in human preferences. In this paper, we consider  $\alpha \sim U(0.55, 0.95)$  and  $\gamma \sim U(0.5, 1.1)$ . These values align with the extensive human experiments in existing research [2], [4], [38], [39]. Parameter  $c_r$  is task-specific and will be identified in our experiments using real human feedback.

### B. Time-Varying Human Stubbornness in Human-robot Coordination

Effective human-robot collaboration requires balancing the robot's objective evaluation with the human's preference to achieve a team decision that enables mutual adaptation. In the context of co-transportation, we consider two modes: either the human follows the robot's guidance or the robot adapts to the human. To model the mode transition, we first introduce a time-varying measure of human stubbornness that quantifies how resistant a human is to deviate from their preferred path option. Then we incorporate it into a mode transition model. When the robot is leading the team, the model also helps to determine which path option the robot should choose that accounts for both the objective cost of the robot and the subjective cost of the human.

1) *Modeling Human Stubbornness*: We define a time-varying stubbornness measure  $\phi(k)$  as follows, where  $k$  denotes the time step,

$$\phi(k) = \phi(0) \cdot \exp\left(\frac{g(k)}{\eta}\right), \quad (11)$$

where

$$g(k) = g(k-1) + \sum_{o \in \mathcal{O}} \omega_o(k) P_o(k), \quad g(0) = 0. \quad (12)$$

Here,  $g(k)$  approximates the accumulation of human discomfort. It grows along the trajectory if the team's movement does not align with human preferences. The accumulation coefficient  $\omega_o(k) \in \{0, 1\}$  is defined such that  $\omega_o(k) = 1$  (not aligned) if the team moves towards an opening,  $\xi$ , that is **not** the next waypoint in option  $o$ ;  $\omega_o(k) = 0$  (aligned), otherwise. Since human preference is unknown and can only be characterized probabilistically, we multiply this coefficient by the probability  $P_o(k)$  from Sec. IV-A.  $P_o(k)$  is repeatedly evaluated at each time step  $k$  using the team's current position as the starting point. Equation (11) then maps the accumulated discomfort  $g(k)$  into human stubbornness  $\phi(k)$  using an exponential function, where  $\phi(0) \in (0, 1]$  is the initial stubbornness of the human, both to be determined. Here, the use of the exponential function is due to the fact that humans exhaust their patience more rapidly as their discomfort accumulates, leading them to become stubborn. A similar exponential function has been used to represent changes in human stubbornness in [17], [40].  $\eta > 0$  is a sensitivity parameter to be identified in our experiments using real human feedback.

2) *Mode Transition Mechanism*: Depending on human stubbornness, we consider two modes during the co-transportation task. The transition of the modes depends on human stubbornness  $\phi(k)$ :

- When  $\phi(k) \leq 1$ , the robot selects a path that actively guides the human.
- When  $\phi(k) > 1$ , the robot adapts to the human.

At the beginning of the task, since  $\phi(0) \in (0, 1]$ , the team starts in robot-leading mode. The system transitions into human-leading mode once the stubbornness measure exceeds 1. In this work, we consider a simple case where the transition occurs only once, i.e., once the human decides to follow their own preference instead of the robot's guidance, the mode remains unchanged until the task is completed. This assumption aligns with our definition that the  $\phi(k)$  in (11) is non-decreasing.

When the system operates in robot-leading mode ( $\phi(k) \leq 1$ ), the robot needs to choose a path that accounts for both the objective cost of the robot and the subjective cost of the human. This is formulated as:

$$o^*(k) = \arg \min_{o \in \mathcal{O}} (1 - \phi(k)) \mathcal{J}_o(k) + \phi(k) \tilde{\mathcal{J}}_o(k) \quad (13)$$

where

$$\tilde{\mathcal{J}}_o(k) = \frac{1}{(\bar{\alpha} - \underline{\alpha})(\bar{\gamma} - \underline{\gamma})} \int_{\alpha} \int_{\gamma} \hat{\mathcal{J}}_o(k | \alpha, \gamma) d\alpha d\gamma. \quad (14)$$

Here, although (6) can evaluate the subject cost of an option  $o$  for any given pair of  $(\alpha, \gamma)$ , the exact human-specific parameters are unknown. Therefore, the human cost for option  $o$  must be approximated over all possible parameters, which yields  $\tilde{\mathcal{J}}_o(k)$ . This  $\tilde{\mathcal{J}}_o(k)$  is repeatedly evaluated at each time step  $k$  using the team's current position as the

starting point. Then in (13), we determine the path option  $o^*(k)$  by weighing the object cost  $\mathcal{J}_o(k)$  and approximated human subjective cost  $\tilde{\mathcal{J}}_o(k)$  based on human stubbornness measure  $\phi(k)$ . This formulation enables a smooth transition between robot-leading and human-leading modes, because before the transition,  $\phi(k) = 1$ , meaning that the cost is dominated by the human's subjective cost. Furthermore, we remark that the path selection problem (13) will not result in locked cycles (i.e., infinite oscillation between options). This is ensured by the monotonic nature of  $\phi(k)$ , and the fact that once the team selects an option  $o^*(k)$ , the corresponding costs  $\mathcal{J}_{o^*}(k)$  and  $\tilde{\mathcal{J}}_{o^*}(k)$  will decrease more than the costs of other options in the next time step. While we do not provide rigorous proof due to space limitations, this statement is also supported by our experimental observations.

When the system operates in human-leading mode ( $\phi(k) > 1$ ), the robot must anticipate possible options the human may choose and adapt its control accordingly. To achieve this, we incorporate a pose optimization strategy, which is introduced in the following subsection.

### C. Pose Optimization in Low-Level Control

In this subsection, we introduce a pose optimization strategy that enhances the robot's (a mobile manipulator) low-level control, enabling it to better anticipate uncertainties in human choices. The pose optimization comes into consideration when the system is operating in human-leading mode.

When the human is leading, the robot does not specifically know which option the human chooses and to mitigate such uncertainties, we exploit the redundancy of the robotic arm, optimizing its joint configuration to remain favorable across all potential path choices, weighted by their probabilities of being chosen by the human.

For a given end-effector trajectory, different joint configurations result in varying control costs. To quantify this, we adopt a receding-horizon Model Predictive Control (MPC) formulation that tracks a nominal trajectory<sup>4</sup> associated with each path option  $o$ . The MPC problem is formulated as:

$$\min_{u^{(0:H-1)}} G_o = \underbrace{\sum_{t=1}^H \|x(t) - s_o(t)\|_Q^2}_{\text{tracking cost}} + \underbrace{\sum_{t=0}^{H-1} \|u(t)\|_R^2}_{\text{control effort}} \quad (15a)$$

$$\text{s.t. } x(t+1) = x(t) + B(q)u(t) \quad (15b)$$

where  $t$  is the MPC time step;  $H$  is the planning horizon;  $s_o(0:H)$  is the nominal trajectory for path option  $o$ ;  $Q$  and  $R$  are weighting matrices for costs, which are positive semi-definite and positive definite, respectively. For a vector  $v$ , and a positive (semi-) definite matrix  $M$ , we let  $\|v\|_M^2 = v^\top M v$ . Equation (15b) represents a generic linearized motion dynamics for the mobile manipulator, where  $x$  denotes the robot's end-effector state, and  $u^{(0:H-1)} = \{u(0), \dots, u(H-1)\}$  denote the control inputs on joints and wheels. A specific example of this model will be used in the

experiment section with details given in the supplementary material [1]. We note that the input matrix  $B(q)$  is linearized from the robot's nonlinear dynamics, which depends on the robot's joint configuration, denoted by  $q$ . Solving (15) yields the optimal cost  $G_o(u^{*(0:H-1)}, q)$  for path option  $o$ , given the joint configuration  $q$ .

As the human may choose any of the options, control decisions should be informed by the costs across all possible options, weighted by their probability distribution  $P_o$  (cf. Section IV-A). To address this, we optimize the joint configuration  $q$ . For a redundant robotic arm, there are infinite feasible poses tracking a nominal trajectory. Direct minimization of  $G_o(u^{*(0:H-1)}, q)$  for optimal  $q$  is intractable due to its complex nonlinear, non-analytic dependence on  $q$ . Instead, we consider a candidate set  $\mathcal{Q}$  of feasible joint configurations and solve the following pose optimization problem:

$$q^* = \arg \min_{q \in \mathcal{Q}} \left\{ \sum_{o \in \mathcal{O}} P_o G_o(u^{*(0:H-1)}, q) + \kappa \|q - q_c\|_2^2 \right\}. \quad (16)$$

For each candidate joint configuration  $q$ , the cost is evaluated across all possible path options  $o$ , weighted by their probability  $P_o$  of human choice. In the second term, we penalize the difference between the current pose  $q_c$  and the new pose  $q$  for pose adjustment, and  $\kappa \in \mathbb{R}_+$  is the cost weight.

By solving for  $q^*$ , the robot proactively prepares for possible human decisions, avoiding singularities, leading to smoother human-robot co-transportation.

## V. SIMULATION RESULTS

In this section, we evaluate the effectiveness of our proposed three modules in a co-transportation task by designing and performing experiments with real human feedback. Then, through simulations, we demonstrate the effectiveness of our models in enhancing task performance with mutual adaptation and pose optimization.

### A. Evaluation of Probability Distribution of Human Choices Model

For the experiment, following our model description, we set  $\alpha \sim \mathcal{U}(0.55, 0.95)$  and  $\gamma \sim \mathcal{U}(0.5, 1.1)$  which captures the range of results from existing literature [2], [4], [38], [39] through extensive human experiments. To implement human probability model (10), we first need to determine  $c_r$  for human subjective cost (6).

**Experiment design:** We create four different environments with different combinations of obstacles and start-target positions, as shown in Fig. 5. The robot's diameter is set as  $d_r = 0.5$  m. In each environment, we consider four reasonable path options to reach the target through different openings, each with varying risk levels and distances. We show these environments to ten human participants and obtain their feedback on how likely they would choose each option in percentages. Participants use visual observation and do not know the objective evaluation of risks and distances.

To determine the  $c_r$  values, we fit the model using the average percentage of the feedback from environments 1-3. The resulting value is  $c_r = 10$ . The model-fitting column of

<sup>4</sup>The trajectory can be generated by existing algorithms [41], [42], which plan motion through openings while avoiding obstacles. Details of trajectory generation are omitted as they are not the main contribution of this paper.



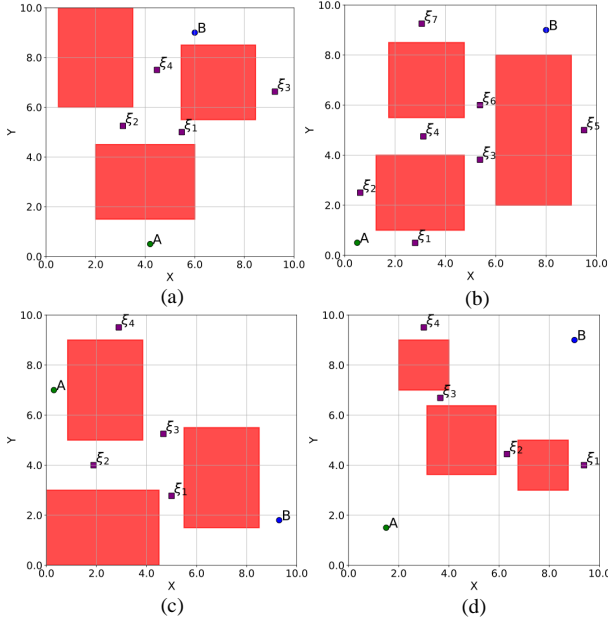


Fig. 5: Start position  $A$ , target position  $B$ . (a) **Environment 1:** Options:  $\{(A, \xi_2, \xi_1, \xi_3, B), (A, \xi_2, \xi_4, B), (A, \xi_1, \xi_4, B), (A, \xi_3, B)\}$ . (b) **Environment 2:** Options:  $\{(A, \xi_2, \xi_4, \xi_6, B), (A, \xi_1, \xi_3, \xi_6, B), (A, \xi_2, \xi_7, B), (A, \xi_1, \xi_5, B)\}$ . (c) **Environment 3:** Options:  $\{(A, \xi_4, B), (A, \xi_2, \xi_1, B), (A, \xi_2, \xi_3, B), (A, \xi_4, \xi_3, \xi_1, B)\}$ . (d) **Environment 4:** Options:  $\{(A, \xi_4, B), (A, \xi_3, B), (A, \xi_2, B), (A, \xi_1, B)\}$ . We use this figure to collect human responses, where the trajectories through openings are not visualized so that participants do not get any extra information.

Table I presents the average percentages provided by humans alongside the corresponding model output (in parentheses) for each option in these three environments.

**Model validation:** We then validate this value by comparing the model's output with the human responses in the fourth environment, where we observe a close alignment in each option.

TABLE I: Probability Distribution of Human Choices.

	Model-Fitting			Validation
	Env 1	Env 2	Env 3	Env 4
<b>Option 1</b>	5 (0)	45 (51.6)	12.5 (5.1)	8 (3.6)
<b>Option 2</b>	45 (39.5)	13.5 (8.7)	30 (35.5)	15 (18.3)
<b>Option 3</b>	40 (36.1)	6.5 (0)	47.5 (59.4)	41 (46.3)
<b>Option 4</b>	10 (24.4)	35 (39.7)	5 (0)	36 (31.8)

Across all environments, we observe that our model can capture the ranking of options in terms of how often that option may be selected. Additionally, for low-probability choices, where humans assigned a small probability to less favorable paths, the model often rounded these probabilities down to zero. This suggests that while the model effectively identifies the most favorable options, it may overlook certain outlier choices. Overall, we found that humans tend to assign higher percentages to relatively safer options, even when this results in longer travel distances.

## B. Evaluation of Time-Varying Human Stubbornness in Human-robot Coordination Model

Here, we evaluate the mode-switching mechanism described in Sec. IV-B. We start by identifying the value  $\eta$  for different participants to implement stubbornness measure (11), then incorporate it into mode transition.

**Experiment design:** We use the environments shown in Fig. 5. For each environment, we create videos of progressively moving trajectories for each path option, representing a robot leading the movement. We show these videos to participants and, during the process, ask them if they want to stop following the robot and switch to another option. If they choose to do so, we record the time at which they provide this feedback. This time corresponds to the mode transition, i.e.,  $\phi(k)$  exceeds 1. We use this time and the trajectory to calculate the individual  $\eta$  for ten participants.<sup>5</sup> Among the ten  $\eta$ , we select three representative ones, corresponding to sensitive ( $\eta = 5$ ), medium ( $\eta = 10.5$ ), and less sensitive ( $\eta = 15$ ) individuals to present the following results.

**Model validation:** To quantitatively evaluate our model, we compare the robot's objective costs (3) with and without the mode transition mechanism across all four environments. For each environment, we randomly sample twenty different  $(\alpha, \gamma)$  values from their respective ranges and compute the average accumulated cost for the resulting human-robot trajectories. These average cost values are presented in Table II.

TABLE II: Average Objective Cost of Human-Robot Coordination under Different Human Stubbornness Sensitivity.

$\eta$	With Model				Without Model			
	Env 1	Env 2	Env 3	Env 4	Env 1	Env 2	Env 3	Env 4
<b>5</b>	1925.38	1895.16	1927.35	2213.82				
<b>10.5</b>	1916.11	1887.75	1853.84	1767.07	1939.67	1962.98	1946.48	2279.98
<b>15</b>	1755.42	1586.56	1826.19	1767.07				

This table shows that across all environments, using the mode transition model with different  $\eta$  values consistently yields lower objective costs for the team compared to not using the model. When  $\eta = 5$ , the mode transition happens early, resulting in slightly lower objective costs than without the model. With  $\eta = 10.5$ , the model yields similar costs in environments 1 and 2 but achieves greater cost reduction in environments 3 and 4. This reflects that by the time the human stubbornness parameter exceeded 1, the human started to prefer the option initially favored by the robot for the team. Furthermore, when  $\eta = 15$ , the robot successfully guides the human to adopt its initially selected path for the team in almost all environments. The results statistically and quantitatively verify the effectiveness of our model in guiding the team toward safer and more efficient path options. It is also worth noting that in all experiments, we do not observe locked cycles when the robot is leading, as discussed in Sec. IV-B.

In addition to cost comparison, we provide a specific example from Environment 4 to illustrate how mutual adaptation enables the robot to influence human decisions and improve the team's behavior. Specifically, in this scenario,

<sup>5</sup>Detail calculations of  $\eta$  are given in the supplementary material.

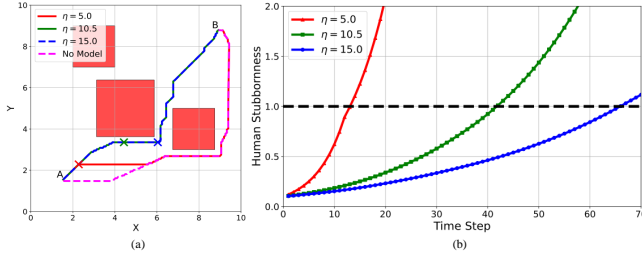


Fig. 6: (a) Trajectories the human-robot team followed during the co-transportation task with  $\eta = 5, 10.5, 15$ , and the trajectory with no mode transition mechanism. The cross ( $\times$ ) marks represent the moment in which the stubbornness parameter exceeds 1, (b) Change in stubbornness over time with different  $\eta$  values.

the robot prefers path option 3 ( $A, \xi_2, B$ ) based on objective evaluation, whereas the human subjectively prefers option 4 ( $A, \xi_1, B$ ) (with the highest probability). We showcase the resulting team trajectory under four cases, assuming the human has three different stubbornness sensitivity  $\eta = 5, 10.5, 15$ , respectively, or when the mode transition mechanism is not applied (i.e., the robot always passively adapts to the human). The corresponding trajectories are shown in Fig. 6-a; the evolution of human stubbornness over time is shown in Fig. 6-b. For  $\eta = 5$ , the human becomes stubborn quickly, which limits the robot’s influence on the team. Consequently, their trajectory almost follows the case without the model transition mechanism, i.e., they follow human preferred path option 4. On the other hand, if  $\eta = 10.5$  or  $15$ , we observed that at a later time (time steps 42, 66, respectively),  $\phi(k)$  exceeds 1, and the robot transitioned to adapt human. However, at this moment, the team’s current position leads the human to change their preference to option 3, as shown in Fig. 6-a. Thus, the team completes the task using this path. This demonstrates that the robot successfully influences human behaviors before they become fully stubborn, ultimately reducing the team’s cost. These results verify the effectiveness of our model. With a gradually increasing human stubbornness parameter and the robot’s mode transition mechanism, the team completes the task using a more efficient path.

### C. Evaluation of Pose Optimization in Low-Level Control

In this subsection, we evaluate the effectiveness of our pose optimization (PO) model to better compensate for varying human uncertainties described in Sec. IV-C.

**Experiment Design:** To obtain the optimized joint configuration  $q^*$ , we generate a set of candidate joint configurations  $\mathcal{Q}$  with the cardinality of fifteen by randomly changing multiple joint angles with a small radian value. For MPC, we set planning horizon  $H = 8$ , weight matrices  $Q = 1000 I_6$  and  $R = I_9$ , and choose  $\kappa = 1$  for pose optimization. To simulate uncertainties, we randomly create four humans with their preference parameters ( $\alpha \pm \omega_\alpha, \gamma \pm \omega_\gamma$ ) defined as sub-ranges of  $\alpha \sim U(0.55, 0.95)$  and  $\gamma \sim U(0.5, 1.1)$ . These parameters may change once or twice during the task, representing shifts in human preferences. The robot utilizes pose optimization to adapt to such changes.

**Model validation:** To validate our model, we define the system’s overall true control cost during the human-leading mode as follows:

$$\mathcal{C} = \sum_{t=1}^T \|x(t) - s(t)\|_Q^2 + \|u(t)\|_R^2 + \kappa \|q - q_c\|_2^2 \quad (17)$$

This equation accumulates true cost over time by considering tracking error, control input, and pose optimization, where  $s$  is the true human state. The robot dynamics follows the form of (15b). In this experiment, we use a Fetch robot with detailed model parameters given in supplementary material [1]. The result is then compared with a baseline where we do not consider pose optimization. For each human in each environment, we conduct 100 random experiments, with the average costs presented in Table III.

TABLE III: Total Robot Control Cost with or without Pose Optimization (PO)

	Environment	$(\alpha, \gamma)$			
		$((0.65 \pm 0.1), (0.6 \pm 0.1))$	$((0.75 \pm 0.2), (0.7 \pm 0.2))$	$((0.8 \pm 0.15), (0.85 \pm 0.15))$	$((0.85 \pm 0.1), (0.95 \pm 0.15))$
With PO	Env 1	843.86	781.47	1546.51	805.34
	Env 2	1267.76	1094.42	1130.03	1162.18
	Env 3	705.26	639.39	1003.86	796.28
	Env 4	760.26	1424.45	822.14	972.99
Without PO	Env 1	1078.35	992.73	1759.19	1315.16
	Env 2	2139.73	1688.07	1180.11	1281.68
	Env 3	732.83	647.08	1200.43	1034.33
	Env 4	890.92	2332.56	1136.61	981.216

As the table indicates, incorporating pose optimization in human-leading mode reduces the system’s true cost in each environment compared to when pose optimization is not used. Notably, although (16) is formulated based on the probability distribution of human choices (i.e., using the overall range of  $\alpha$  and  $\gamma$ , rather than the sub-ranges, which are assumed to be unknown to robots), the resulting optimized joint configuration proves beneficial when collaborating humans with varying preference parameters. These results demonstrate that pose optimization, along with the proposed framework, enhances overall task performance, ensuring safety and efficiency.

## VI. CONCLUSION

In this paper, we introduced a framework to address two main challenges in human-robot co-transportation without direct communication: the uncertainty of human preference parameters, and the need to balance adaptation strategies that benefit both humans and robots. We derived a model that captures the probability distribution of human choices rather than relying on fixed parameters. We then integrated a time-varying stubbornness measure to analyze the mode transition among human-robot coordination. Following these, we proposed a pose optimization strategy for the robot’s low-level control to mitigate choice uncertainties when the human is leading. We validated our framework through experiments with human participants, one to gather preference data and another to capture the stubbornness parameter. Then, we further demonstrated how the integrated mode transition model and pose optimization technique enhanced overall task efficiency and safety. Future work will include additional human factors (e.g. fatigue, stress) and extend to multi-human multi-robot co-transportation scenarios.

## REFERENCES

- [1] A. J. Mahmud, W. Li, and X. Wang, "Supplementary: Mutual adaptation in human-robot co-transportation with human preference uncertainty," [https://mason.gmu.edu/~xwang64/papers/25\\_IROS\\_HRCT\\_Supp.pdf](https://mason.gmu.edu/~xwang64/papers/25_IROS_HRCT_Supp.pdf).
- [2] A. Tversky and D. Kahneman, "Advances in prospect theory: Cumulative representation of uncertainty," *Journal of Risk and uncertainty*, vol. 5, pp. 297–323, 1992.
- [3] M. Guirao, "Subjective scaling of length and area and the matching of length to loudness and brightness.," *Journal of Experimental Psychology*, vol. 66, no. 2, p. 177, 1963.
- [4] D. Prelec, "The probability weighting function," *Econometrica*, pp. 497–527, 1998.
- [5] M. Fintz, M. Osadchy, and U. Hertz, "Using deep learning to predict human decisions and using cognitive models to explain deep learning models," *Scientific reports*, vol. 12, no. 1, p. 4736, 2022.
- [6] A. Gorgan Mohammadi and M. Ganjtabesh, "On computational models of theory of mind and the imitative reinforcement learning in spiking neural networks," *Scientific Reports*, vol. 14, no. 1, p. 1945, 2024.
- [7] B. Sadrifaridpour, H. Saedi, J. Burke, K. Madathil, and Y. Wang, "Modeling and control of trust in human-robot collaborative manufacturing," *Robust intelligence and trust in autonomous systems*, pp. 115–141, 2016.
- [8] S. Nikolaidis, D. Hsu, and S. Srinivasa, "Human-robot mutual adaptation in collaborative tasks: Models and experiments," *The International Journal of Robotics Research*, vol. 36, no. 5-7, pp. 618–634, 2017.
- [9] L. Peternel, N. Tsagarakis, D. Caldwell, and A. Ajoudani, "Robot adaptation to human physical fatigue in human-robot co-manipulation," *Autonomous Robots*, vol. 42, pp. 1011–1021, 2018.
- [10] D. Sirintuna, A. Giammarino, and A. Ajoudani, "An object deformation-agnostic framework for human-robot collaborative transportation," *IEEE Transactions on Automation Science and Engineering*, vol. 21, no. 2, pp. 1986–1999, 2023.
- [11] N. Feng, X. Guo, X. Yu, S. Zhang, and W. He, "Human-robot sharing operation in co-transporting for nonholonomic mobile robot," *IEEE Transactions on Cognitive and Developmental Systems*, 2024.
- [12] E. Noohi, M. Žefran, and J. L. Patton, "A model for human-human collaborative object manipulation and its application to human-robot interaction," *IEEE transactions on robotics*, vol. 32, no. 4, pp. 880–896, 2016.
- [13] M. S. Tomov, E. Schulz, and S. J. Gershman, "Multi-task reinforcement learning in humans," *Nature Human Behaviour*, vol. 5, no. 6, pp. 764–773, 2021.
- [14] R. Ratcliff and G. McKoon, "The diffusion decision model: theory and data for two-choice decision tasks," *Neural computation*, vol. 20, no. 4, pp. 873–922, 2008.
- [15] V. M. Eguíluz, N. Masuda, and J. Fernández-Gracia, "Bayesian decision making in human collectives with binary choices," *PLoS One*, vol. 10, no. 4, p. e0121332, 2015.
- [16] S. Prabhudesai, L. Yang, S. Asthana, X. Huan, Q. V. Liao, and N. Banovic, "Understanding uncertainty: how lay decision-makers perceive and interpret uncertainty in human-ai decision making," in *Proceedings of the 28th international conference on intelligent user interfaces*, pp. 379–396, 2023.
- [17] T. Heskes, "The use of being stubborn and introspective," in *Prerational Intelligence: Adaptive Behavior and Intelligent Systems Without Symbols and Logic, Volume 1, Volume 2 Prerational Intelligence: Interdisciplinary Perspectives on the Behavior of Natural and Artificial Systems, Volume 3*, pp. 1184–1200, Springer, 2000.
- [18] A. J. Mahmud, D. M. Nguyen, F. Veiga, X. Xiao, and X. Wang, "Human uncertainty-aware mpc for enhanced human-robot collaborative manipulation," in *2024 IEEE 7th International Conference on Industrial Cyber-Physical Systems (ICPS)*, pp. 1–6, 2024.
- [19] B. Akgun, M. Cakmak, J. W. Yoo, and A. L. Thomaz, "Trajectories and keyframes for kinesthetic teaching: A human-robot interaction perspective," in *Proceedings of the seventh annual ACM/IEEE international conference on Human-Robot Interaction*, pp. 391–398, 2012.
- [20] A. Kanazawa, J. Kinugawa, and K. Kosuge, "Adaptive motion planning for a collaborative robot based on prediction uncertainty to enhance human safety and work efficiency," *IEEE Transactions on Robotics*, vol. 35, no. 4, pp. 817–832, 2019.
- [21] M. Wu, B. Taetz, E. D. Saraiva, G. Bleser, and S. Liu, "On-line motion prediction and adaptive control in human-robot handover tasks," in *2019 IEEE International Conference on Advanced Robotics and its Social Impacts (ARSO)*, pp. 1–6, IEEE, 2019.
- [22] A. Bolu and Ö. Korçak, "Adaptive task planning for multi-robot smart warehouse," *IEEE Access*, vol. 9, pp. 27346–27358, 2021.
- [23] B. P. E. A. Vásquez and F. Matía, "A tour-guide robot: Moving towards interaction with humans," *Engineering Applications of Artificial Intelligence*, vol. 88, p. 103356, 2020.
- [24] S. Cai, A. Ram, Z. Gou, M. A. W. Shaikh, Y.-A. Chen, Y. Wan, K. Hara, S. Zhao, and D. Hsu, "Navigating real-world challenges: A quadruped robot guiding system for visually impaired people in diverse environments," in *Proceedings of the 2024 CHI Conference on Human Factors in Computing Systems*, pp. 1–18, 2024.
- [25] E. M. Van Zoelen, E. I. Barakova, and M. Rauterberg, "Adaptive leader-follower behavior in human-robot collaboration," in *2020 29th IEEE International Conference on Robot and Human Interactive Communication (RO-MAN)*, pp. 1259–1265, IEEE, 2020.
- [26] M. Kwon, E. Biyik, A. Talati, K. Bhasin, D. P. Losey, and D. Sadigh, "When humans aren't optimal: Robots that collaborate with risk-aware humans," in *Proceedings of the 2020 ACM/IEEE international conference on human-robot interaction*, pp. 43–52, 2020.
- [27] R. Kumar, V. Som, and N. Yao, "Sequential transfer learning-based human decision making model for human-robot co-learning and insights from user feedback analysis," in *2024 33rd IEEE International Conference on Robot and Human Interactive Communication (ROMAN)*, pp. 250–257, IEEE, 2024.
- [28] M. Hsu, M. Bhatt, R. Adolphs, D. Tranel, and C. F. Camerer, "Neural systems responding to degrees of uncertainty in human decision-making," *Science*, vol. 310, no. 5754, pp. 1680–1683, 2005.
- [29] A. R. Bland and A. Schaefer, "Different varieties of uncertainty in human decision-making," *Frontiers in neuroscience*, vol. 6, p. 85, 2012.
- [30] P. C. Trimmer, A. I. Houston, J. A. Marshall, M. T. Mendl, E. S. Paul, and J. M. McNamara, "Decision-making under uncertainty: biases and bayesians," *Animal cognition*, vol. 14, pp. 465–476, 2011.
- [31] J. G. Johnson and J. R. Busemeyer, "Decision making under risk and uncertainty," *Wiley Interdisciplinary Reviews: Cognitive Science*, vol. 1, no. 5, pp. 736–749, 2010.
- [32] J. Cavacanti Santos and M. Martins da Silva, "Redundancy resolution of kinematically redundant parallel manipulators via differential dynamic programming," *Journal of Mechanisms and Robotics*, vol. 9, no. 4, p. 041016, 2017.
- [33] H. Kim, L. M. Miller, N. Byl, G. M. Abrams, and J. Rosen, "Redundancy resolution of the human arm and an upper limb exoskeleton," *IEEE transactions on biomedical engineering*, vol. 59, no. 6, pp. 1770–1779, 2012.
- [34] L. Huo and L. Baron, "The joint-limits and singularity avoidance in robotic welding," *Industrial Robot: An International Journal*, vol. 35, no. 5, pp. 456–464, 2008.
- [35] H. Cheong, M. Ebrahimi, and T. Duggan, "Optimal design of continuum robots with reachability constraints," *IEEE Robotics and Automation Letters*, vol. 6, no. 2, pp. 3902–3909, 2021.
- [36] A. J. Mahmud, A. H. Raj, D. M. Nguyen, X. Xiao, and X. Wang, "Human-robot co-transportation with human uncertainty-aware mpc and pose optimization," *arXiv preprint arXiv:2404.00514*, 2024.
- [37] S. S. Stevens, "On the psychophysical law.," *Psychological review*, vol. 64, no. 3, p. 153, 1957.
- [38] B. J. Thomas, S. Heiden, K. Dyson, M. Bartz, J. Curtin, and V. Zbotaniw, "The psychophysics of affordance perception: Stevens' power law scaling of perceived maximum forward reachability with an object," *Attention, Perception, & Psychophysics*, vol. 85, no. 8, pp. 2869–2878, 2023.
- [39] M. Abdellaoui, H. Bleichrodt, and C. Paraschiv, "Loss aversion under prospect theory: A parameter-free measurement," *Management science*, vol. 53, no. 10, pp. 1659–1674, 2007.
- [40] Y. Tian, P. Jia, A. Mirtabatabaei, L. Wang, N. E. Friedkin, and F. Bullo, "Social power evolution in influence networks with stubborn individuals," *IEEE Transactions on Automatic Control*, vol. 67, no. 2, pp. 574–588, 2021.
- [41] P. E. Hart, N. J. Nilsson, and B. Raphael, "A formal basis for the heuristic determination of minimum cost paths," *IEEE transactions on Systems Science and Cybernetics*, vol. 4, no. 2, pp. 100–107, 1968.
- [42] C. W. Warren, "Fast path planning using modified a\* method," in *[1993] Proceedings IEEE International Conference on Robotics and Automation*, pp. 662–667, IEEE, 1993.